Research on a Prediction Model for Shared Bicycles Based on Ceemdan-ipso-lstm

Qi Zhou, Jinbao Zhao, Keke Hou, Wenjing Liu, Jiawei Jiang, Mingxing Li

Abstract—**Shared bicycles, as an important mode of urban short-distance travel, play a significant role in enhancing traffic efficiency, alleviating traffic congestion and promoting sustainable mobility. However, the temporal and spatial volatility of shared bicycle demand makes it difficult to achieve efficient dispatch balance during peak travel hours, which has become one of the key factors restricting its rapid development. A high-precision shared bicycle demand prediction model, the CEEMDAN-IPSO-LSTM model, has been constructed to address issues such as low bicycle turnover efficiency and imbalanced supply and demand. It eliminates noise from time series data via adaptive noise complete ensemble empirical mode decomposition (CEEMDAN). This model integrates improved particle swarm optimization (IPSO) to dynamically optimize the hyperparameters of the long short-term memory network (LSTM). Moreover, it adopts an independent prediction strategy among components to enhance the model's prediction accuracy. Experimental results indicate that, in comparison with traditional LSTM, PSO-LSTM, IPSO-LSTM, and CEEMDAN-LSTM models, the constructed model exhibits the best performance in terms of error metrics, including mean absolute error (MAE), root mean square error (RMSE), and the coefficient of determination (R^2). This fully demonstrates its superiority in prediction accuracy and stability.**

Index Terms—**shared bicycles, demand prediction, empirical mode decomposition, improved particle swarm optimization, long short-term memory network**

I. Introduction

THE emergence of bike-sharing systems has significantly transformed urban mobility by bridging the gap between public transportation and final destinations, thereby reducing reliance on private cars, taxis, and ride-hailing services [1], [2]. This innovation has not only mitigated urban traffic congestion but also curbed greenhouse gas emissions, making a significant contribution to the sustainable development goals. Statistical data indicate that over 700 bike-sharing systems are currently in operation across various countries globally, and the utilization of shared bicycles is steadily expanding [3]. Nevertheless, enhancing operational efficiency remains a crucial challenge. There is a pressing need for advanced predictive models to determine the optimal number of vehicles and spatial distribution strategies [4]. Accurate demand forecasting and well-planned infrastructure are essential for maximizing the socioeconomic and ecological advantages of bike-sharing systems, while simultaneously minimizing operational inefficiencies, such as improper parking and resource redundancy [5], [6].

Regarding the prediction method, the experimental findings indicate that the decomposition clustering ensemble (DCE) learning approach proposed by Wei et al. [7] can significantly enhance the prediction accuracy. To account for the spatio-temporal correlations, Lv et al. [8] employed a stacked autoencoder (SAE) model to characterize the traffic flow features for prediction purposes and constructed a traffic flow prediction model grounded in deep learning. The LSTM is an improvement and extension of recurrent neural network (RNN) [9]. Cai et al. [10] utilized the LSTM model to predict the future trajectory of the underwater vehicle-manipulator system (UVMS) and put forward a novel prediction framework based on nonlinear model predictive control (NMPC). Given that the hidden variables in LSTM lack the representation of high-quality data, a supervised LSTM (SLSTM) network was proposed for soft sensing techniques [11]. Huang et al. [12] applied the CNN-LSTM-Attention model in wind speed prediction.

In the field of shared bicycle demand forecasting, researchers have proposed various methods to address the complex spatio-temporal characteristics of bicycles. For example, Qiao et al. [13] presented a three-in-one dynamic shared bicycle demand forecasting model, which was developed in response to the complex demand for bicycles under non-classical circumstances. This model combines three core technologies: station clustering, dynamic factors, and LSTM network prediction. Wang et al. [14] initiated their research from geographical and spatial perspectives. They analyzed the influence of non-motorized transportation facilities, intersection density, and land use on bicycle demand and employed a multi-scale geographically weighted regression (MGWR) model for demand prediction. Building on this, Feng et al. [15] proposed a novel

Manuscript received May 10, 2025; revised July 19, 2025. This work was supported by the National Natural Science Foundation of China under Grant 51608313 and the General Project of Shandong Natural Science Foundation under Grant ZR2021MF109.

Qi Zhou is a graduate student at the School of Transportation and Vehicle Engineering, Shandong University of Technology, Zibo, 255000 China (e-mail: zhouqi919@126.com).

Jinbao Zhao is an associate professor at the School of Transportation and Vehicle Engineering, Shandong University of Technology, Zibo, 255000 China (corresponding author to provide phone: 156-5032-1793; e-mail: zhaojinbao919@163.com).

Keke Hou is a graduate student at the School of Transportation and Vehicle Engineering, Shandong University of Technology, Zibo, 255000 China (e-mail: 1727268517@qq.com).

Wenjing Liu is a graduate student at the School of Transportation and Vehicle Engineering, Shandong University of Technology, Zibo, 255000 China (e-mail: wangyannian02@163.com).

Jiawei Jiang is a graduate student at the School of Transportation and Vehicle Engineering, Shandong University of Technology, Zibo, 255000 China (e-mail: 2195018162@126.com).

Mingxing Li is a graduate student at the School of Transportation and Vehicle Engineering, Shandong University of Technology, Zibo, 255000 China (e-mail: z15650321793@foxmail.com).

spatio-temporal aggregation graph neural network (STAGNN) to overcome the limitations of existing models in capturing the dynamic characteristics of bicycle flows. Additionally, Hong [16] carried out time series clustering analysis to categorize 263 shared bicycle stations in the four major entrance areas of central Seoul and constructed a random forest regression model to precisely predict the demand at each station. Continuing this line of research, Shi et al. [17] utilized the shared bicycle data in London as the dataset and applied LSTM neural network models as well as machine learning models grounded on meteorological and temporal factors to forecast the hourly demand for shared bicycles. Given that the utilization of shared bicycles is influenced by numerous diverse factors, accurately predicting the quantity of shared bicycles poses a challenge. To address this critical issue, Huang et al. [18] put forward a bimodal gaussian non-homogeneous poisson (BGIP) algorithm for forecasting shared bicycle demand. Moreover, to enhance the service quality of bike-sharing systems (BSSs) and resolve the problem of uneven distribution of bike-sharing space, Ashqar et al. [19] proposed a novel spatial prediction model during the search for new stations. Finally, Ma et al. [20] presented a CNN-LSTM-Attention prediction model based on the traffic flow prediction theory to accomplish precise demand forecasting for shared bicycles.

Despite the fact that certain scholars have carried out relevant research on the demand prediction of shared bicycles, the issue of matching bicycle usage with demand across stations remains to be further investigated. This is particularly the case during peak hours when the borrowing and returning volumes exhibit significant fluctuations. To scientifically establish the dispatch frequency and quantity, it is essential to conduct a thorough analysis of the borrowing and returning demand characteristics of stations. This analysis can optimize resource allocation and enhance system efficiency. In this chapter, a demand forecasting method for shared bicycles based on the CEEMDAN-IPSO-LSTM model is explored. The objective is to construct an accurate and efficient forecasting model that can capture the dynamic characteristics of demand.

II. Model Construction

A. Model framework construction

In the integrated model for forecasting urban shared bicycle demand, removing random noise from prediction data and optimizing neural network parameters are crucial to tackle the complexity and non-stationarity of time-series data. First, CEEMDAN is employed to decompose time-series data into multiple intrinsic mode functions (IMFs) of varying frequencies and complexities, together with a residual component (Res), which lays the foundation for noise elimination. Next, the IPSO algorithm is introduced to dynamically adjust LSTM parameters [21]—such as the number of neurons, learning rate, and iteration count—thereby enhancing the model's adaptability to nonlinear patterns. This sequential integration of CEEMDAN decomposition and IPSO optimization facilitates the establishment of the CEEMDAN-IPSO-LSTM model, whose operational flowchart is depicted in Fig. 1.

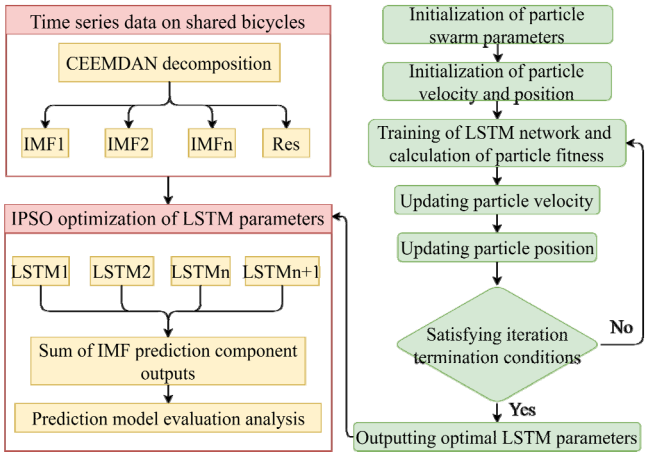

Fig. 1. CEEMDAN-IPSO-LSTM Prediction Model Flowchart

B. CEEMDAN-IPSO-LSTM Prediction Model Flowchart

Adaptive noise complete ensemble empirical mode decomposition (CEEMDAN) represents an adaptive posterior decomposition approach that has been enhanced based on empirical mode decomposition (EMD) and ensemble empirical mode decomposition (EEMD). This method is capable of adaptively decomposing the given data into multiple mode components [24]. By adaptively introducing opposite white noise to the original signal, CEEMDAN effectively circumvents the problems of mode mixing in EMD and reconstruction errors in EEMD decomposition after the addition of white noise [25]. The decomposition steps of CEEMDAN are as follows:

Let $G_i(\cdot)$ denote the i-th IMF mode component obtained after EMD decomposition of the sequence, ε_i be the noise coefficient added by CEEMDAN to the input sequence at the i-th stage, and $c_m(t)$ denote the m-th IMF component generated by the CEEMDAN algorithm at a certain stage. Add N instances of Gaussian white noise to the original signal $y(t)$ to generate N preprocessed sequences $y_n(t)$ (n=1, 2, …, N).

$$y_n(t) = y(t) + \varepsilon_0 \delta_n(t) \tag{1}$$

In the equation, ε_0 is the noise weighting coefficient, and $\delta_n(t)$ is the n-th addition of Gaussian white noise.

Perform modal decomposition on the $y_n(t)$ sequence, extract the first IMF component, and calculate its mean value, which is the first component $c_1(t)$ obtained from the CEEMDAN decomposition. Simultaneously, obtain the first sequence $r_1(t)$, which is the residual, as shown in (2) and (3).

$$c_1(t) = \frac{1}{N}\sum_{1}^{N} c_1^n(t), n = \{1,2,...,N\} \tag{2}$$

$$r_1(t) = y(t) - c_1(t) \tag{3}$$

Gaussian white noise is added to the residual sequence $r_1(t)$ to construct N new sequences. Modal decomposition is then continued to compute their mean values, yielding the next modal component $c_2(t)$, as described in (4). Subtracting $c_2(t)$ from the residual sequence results in $r_2(t)$, as shown in (5).

$$c_2(t) = \frac{1}{N}\sum_{1}^{N} E_1\left(r_1(t) + \varepsilon_1 E_1\left(\delta_n(t)\right)\right), n = \{1,2,...,N\} \tag{4}$$

$$r_2(t) = r_1(t) - c_2(t) \tag{5}$$

Repeat the above steps, and the residual formula for stage

m is shown in (6).

$$r_m(t) = r_{m-1}(t) - c_m(t) \tag{6}$$

Continue performing N modal decompositions to obtain the $(m+1)$-th sequence, as shown in (7). By following this recursive process, the decomposition continues until the final residual sequence is obtained, ultimately yielding (8) upon completion of the signal decomposition.

$$c_{m+1}(t) = \frac{1}{N}\sum_{1}^{N} E_1\left(r_m(t) + \varepsilon_m E_m\left(\delta_n(t)\right)\right), n = \{1,2,...,N\} \tag{7}$$

$$y(t) = R(t) + \sum_{1}^{M} c_m(t) \tag{8}$$

C. Long short-term memory network (LSTM)

Long short-term memory network (LSTM) is an extension of RNNs [26] specifically designed to address the gradient vanishing and gradient explosion issues encountered by traditional RNNs when processing sequential data. LSTM achieves this by introducing a gating mechanism (input gate, forget gate, and output gate), which effectively controls the flow and update of information, enabling long-term information transmission and persistence across different time steps [27].

The forget gate and input gate collaborate to manage the cell state. The forget gate outputs a vector of values between 0 and 1, selectively discarding information from the previous cell state. Concurrently, the input gate decides which elements from the current input and candidate cell state should be added to update the cell state. By controlling information retention and addition, these two gates update the cell state at each time step, refining it further with candidate cells to preserve only relevant information. Subsequently, the output gate processes the updated cell state, generating a vector that determines the hidden state and controls the information flow to the next layer, serving as the final output of the LSTM unit.

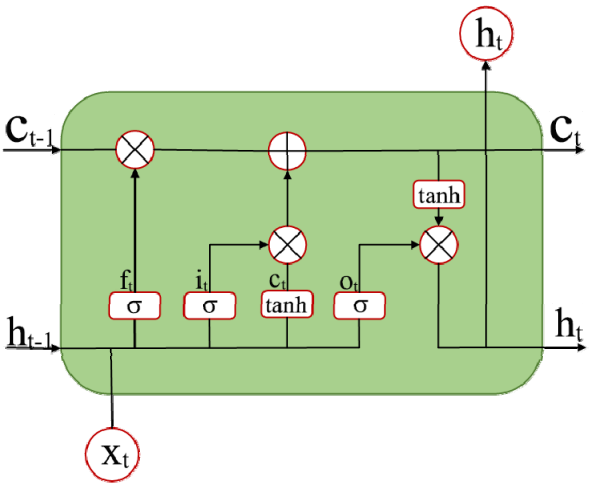

Fig. 2. LSTM Process Flow Diagram

As shown in the Fig. 2, a typical LSTM neural network is composed of an input layer, an output layer, and a hidden layer. The storage units in the hidden layer consist of input gates i_t, output gates o_t, and forget gates f_t, which are used to control the unit state. The forget gate f_t determines which information to delete from the unit state C_{t-1} at the previous moment.

D. Improved particle swarm optimization (IPSO)

Particle swarm optimization (PSO) has been widely applied in various fields such as neural network optimization, image processing, decision scheduling, machine learning, and data mining [28]. However, the traditional PSO algorithm uses inertial weights ω and learning factors c_1 and c_2, which are typically set as constants. This leads to drawbacks such as premature convergence, insufficient global convergence capability, low search efficiency in later iterations, and poor accuracy. When the inertial weight ω is too large, particles may move too far during iterations, leading to missing the optimal solution or causing iterative convergence oscillations. Conversely, when ω is too small, the iterative step size becomes too small, resulting in slow convergence and the inability to reach the optimal solution. To address these issues, a linearly decreasing inertial weight ω is adopted to improve the initial global search efficiency of particles. As the number of iterations increases, the inertial weight ω is gradually reduced to enhance the local search capability of particles in the solution space and achieve more precise local search in the later stages of the solution process. The inertial weight ω is expressed as:

$$\omega_k = \omega_{\max} - \frac{(\omega_{\max} - \omega_{\min})k}{G_{\max}} \tag{9}$$

In the formula, ω_k represents the inertial weight at the k-th iteration; ω_{min} and ω_{max} denote the maximum and minimum values of the inertial weight settings, respectively; G_{max} denotes the maximum number of iterations. Its characteristic is that the inertial coefficient dynamically adjusts according to the state of the particle swarm. When the values of the particle swarm tend to be consistent, ω increases; when the particle swarm disperses, ω decreases. This promotes global search, thereby balancing the global search speed and local search accuracy. The c_1 and c_2 are:

$$c_{1,k} = c_{1,\max} - \frac{(c_{1,\max} - c_{1,\min})k}{G_{\max}} \tag{10}$$

$$c_{2,k} = c_{2,\min} - \frac{(c_{2,\max} - c_{2,\min})k}{G_{\max}} \tag{11}$$

$c_{1,k}$ and $c_{2,k}$ denote the learning factors at the kth iteration; $c_{1,max}$ and $c_{1,min}$ denote the maximum and minimum values of c_1, respectively; $c_{2,max}$ and $c_{2,min}$ denote the maximum and minimum values of c_2, respectively; G_{max} denotes the maximum number of iterations.

To demonstrate the superiority of the IPSO algorithm, this study selected four classic benchmark functions to compare PSO and IPSO, focusing on evaluating the advantages of IPSO in terms of global search capability, convergence speed, and solution accuracy, and verifying its effectiveness in complex optimization problems [29]. The Sphere function was used to examine convergence speed, the Rosenbrock function to test global search capability, while the Rastrigin and Griewank functions assess the ability to escape local optima. To ensure fairness, the population size for all algorithms was set to 30, and the maximum number of iterations was set to 100. The performance comparison results of the benchmark functions are shown in Fig. 3.

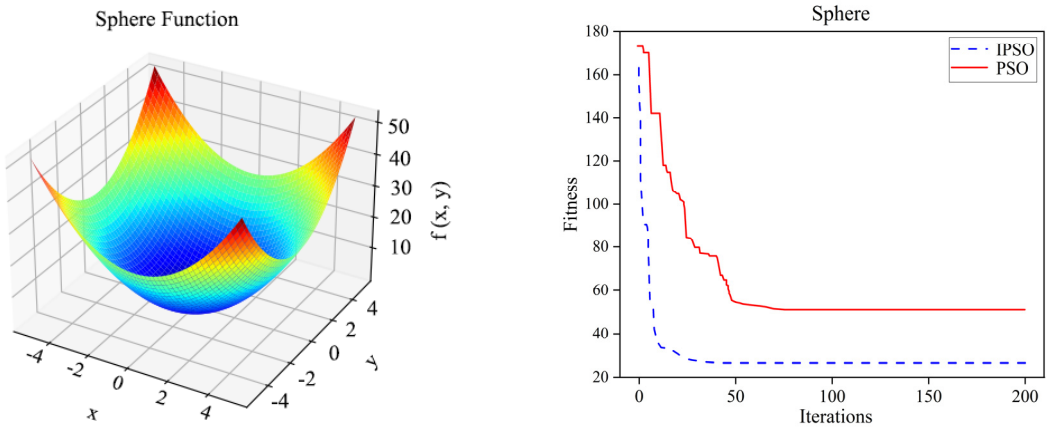

(a) Sphere function performance test comparison

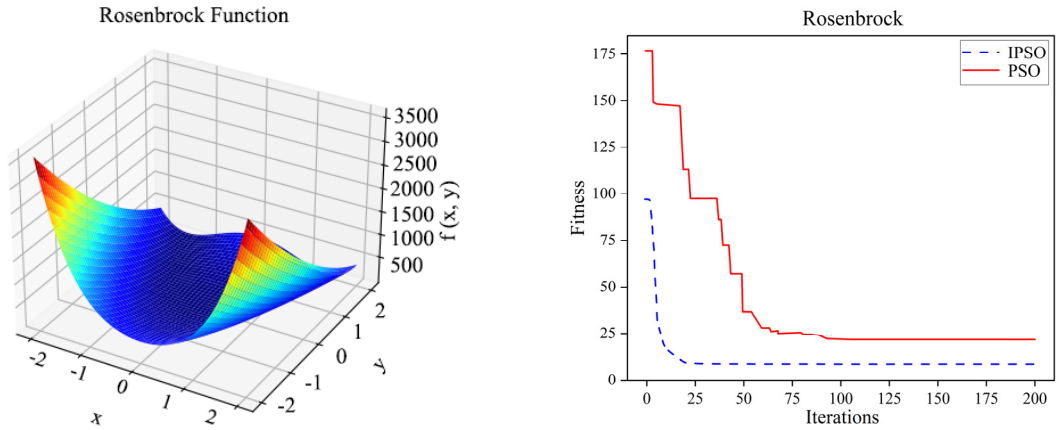

(b) Rosenbrock function performance comparison

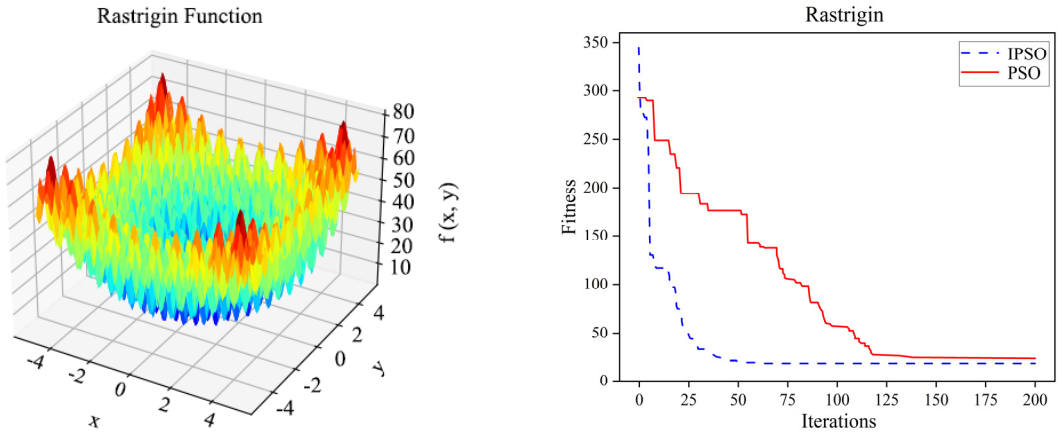

(c) Rastrigin function performance comparison

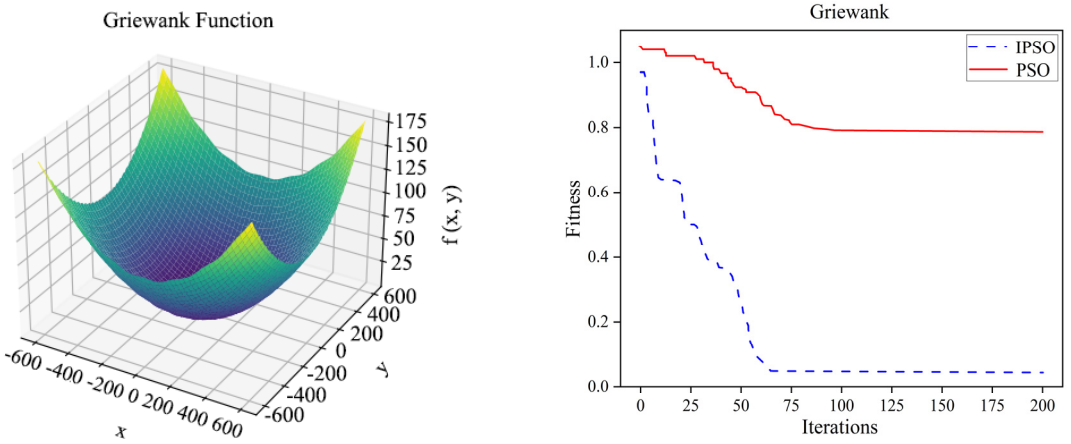

(d) Comparison of Griewank function performance tests

Fig. 3. Benchmark function performance comparison results

III. Case Study

A. Data set selection

The experimental data for this study were obtained from the Kaggle website (https://www.kaggle.com/datasets) and consist of bicycle trip data from Citi Bike in New York City. A total of 1.06 million bicycle trip records were extracted on an hourly basis from July 1 to 31, 2023. The study considered the impact of time-related features (hour, weekday, and holiday) and weather-related features (temperature, wind speed and precipitation) on the demand for shared bicycles. By integrating these multi-dimensional features, a multivariate time-series prediction model was developed to provide a more robust basis for operational scheduling and resource allocation in shared bicycle systems.

Using the shared bicycles station distribution data and the number of bicycles parked at each station obtained from the official website of the New York City government (https://www.nyc.gov), a visualization analysis of the bicycle supply and demand situation at each station was conducted. According to the availability status of the bicycles, each station is color-coded as shown in Fig. 4. Specifically, red represents the absence of available bicycles at the station; yellow indicates that a limited number of bicycles are available, which can partially satisfy the demand but the supply is insufficient; and green denotes that an adequate number of bicycles are available to meet the riding requirements of users.

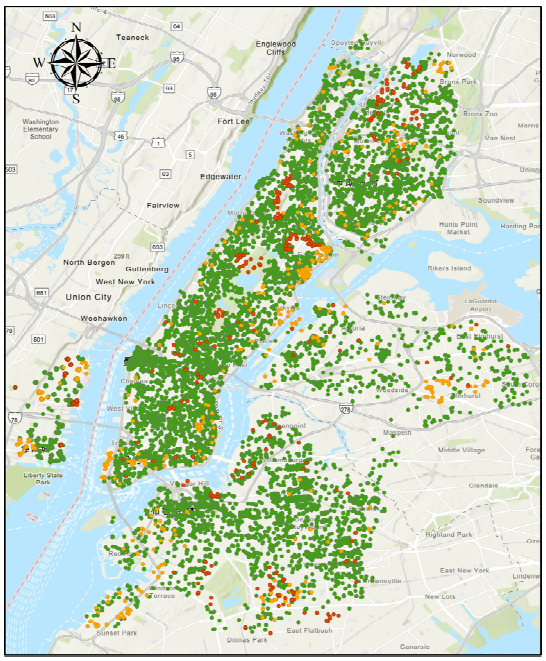

Fig. 4. Shared bicycles station status

B. Model parameter optimization

To assess the superiority and prediction accuracy of the CEEMDAN-IPSO-LSTM hybrid model, this study performs a comprehensive comparative analysis against benchmark models including LSTM [30], PSO-LSTM [13], IPSO-LSTM [14], and CEEMDAN-LSTM.

1) Initialize particle swarm parameters

To determine the population size, number of iterations, learning factors, and value ranges for particle positions and velocities, the following specific parameter settings are adopted: the number of particles is set to PN = 50, the number of iterations is 200, and the search dimension is 8. The weighting factors are defined as ω_{max} = 0.9, ω_{min} = 0.4, with learning factors c_1 = 2, c_2 = 2, and random coefficients r_1 = 0.8, r_2 = 0.3. Particles are initialized by randomly generating a particle vector $Xi=(n, l_r, h_1, h_2)$, where: n denotes the algorithm iteration count (ranging between 10 and 100), l_r represents the learning rate (ranging between 0.001 and 0.01), and h_1 and h_2 denote the number of neurons in the first and second hidden layers, respectively (both ranging between 1 and 100). The particle velocity $V_i = (V_{i1}, V_{i2}, V_{i3}, V_{i4})$ is generated using uniformly distributed random samples within the interval [0, 1), as described in [14].

TABLE I
PSO and IPSO Parameter Settings

	PSO parameter values	IPSO parameter values
Number of particles	50	50
Number of iterations	200	200
Search dimension	8	8
Weight inertia	ω_{max}=0.9 ω_{min}=0.4	ω_{max}=0.9 ω_{min}=0.4
Learning factor	$c_{1,max}$=2 $c_{1,min}$=0.5 $c_{2,max}$=2 $c_{2,min}$=0.5	$c_{1,max}$=2 $c_{1,min}$=0.5 $c_{2,max}$=2 $c_{2,min}$=0.5

2) Update particle positions and velocities

The fitness function is defined to evaluate the performance of parameter combinations for each particle. It quantifies the model's error or performance metric on the validation set, as shown in (12):

$$fit = \frac{1}{n}\Sigma\left(y' - y\right)^2 \tag{12}$$

In the formula: n denotes the the number of prediction sample points, y' represents the actual output of the sample points, and y is the expected output of the same sample points.

During each iteration, the position of each particle and its fitness value are computed. By comparing the latest fitness value with the initial fitness value of the particle's position, the optimal individual position and subsequently the optimal population position are determined. In each iteration, particles update their velocity and position based on the fitness function to continuously optimize the search process. Through updating the optimal individual positions and the global optimal position, particles gradually converge to the optimal solution. Within the maximum number of iterations, particle positions are continuously adjusted, and the optimal particle is finally output, representing the optimal parameters of the LSTM neural network.

In the IPSO-LSTM, PSO-LSTM, and CEEMDAN-IPSO-LSTM models, the corresponding optimization algorithms dynamically determine the number of neurons in the hidden layer. The optimization results of the particle swarm algorithm are shown in TABLE II, and those of the CEEMDAN-IPSO-LSTM are listed in TABLE III.

C. Evaluation criteria selection

These metrics include mean absolute error (MAE), root mean square error (RMSE), mean absolute percentage error (MAPE), and coefficient of determination (R^2) [15].

$$MAE = \frac{1}{n}\sum_{i=1}^{n} | y_i - y_i | \tag{13}$$

$$RMSE = \sqrt{\frac{1}{n}\sum_{i=1}^{n}\left(y_i - y_i\right)^2} \tag{14}$$

$$MAPE = \frac{1}{n}\sum_{i=1}^{n}\left|\frac{y_i - y_i}{y_i}\right| \times 100\% \tag{15}$$

$$R^2 = \frac{1-\sum_{r=1}^{N}\left(x_r - \hat{x}_r\right)^2}{\sum_{r=1}^{N}\left(x_r - \overline{x}_r\right)^2} \tag{16}$$

In the formula, x_r represents the actual demand data for a single vehicle, $\hat{x}_r$ represents the predicted demand value for a single vehicle, and $\overline{x}_r$ represents the predicted average value.

TABLE IV
LSTM PARAMETER SETTINGS

Parameter Name	Parameter Value	Parameter Name	Parameter Value
Time step	12	Loss function	MSE
Number of hidden layers	2	Epoch	100
Optimization function	*Adam*	Batch size	32
Activation function	*Sigmoid*	Dropout	0.2

TABLE II
PARAMETER OPTIMIZATION RESULTS OF PARTICLE SWARM OPTIMIZATION ALGORITHM

IMF	IPSO-LSTM				PSO-LSTM			
	Number of iterations	Learning rate	Hidden layer 1	Hidden layer 2	Number of iterations	Learning rate	Hidden layer 1	Hidden layer 2
IMF1	184	0.0056	159	24	154	0.0041	105	21
IMF2	175	0.0061	121	81	114	0.0021	114	19
IMF3	192	0.0081	239	16	144	0.0084	144	8
IMF4	177	0.0031	147	73	135	0.0031	135	16
IMF5	202	0.0011	167	27	150	0.0074	150	6
IMF6	182	0.0036	146	33	118	0.0061	18	25
IMF7	184	0.0051	194	19	104	0.0081	104	31
IMF8	176	0.0071	144	91	121	0.0067	121	22
Res	182	0.0014	139	67	110	0.0039	110	28

TABLE III
PARAMETER OPTIMIZATION RESULTS OF CEEMDAN-IPSO-LSTM

IMF	CEEMDAN-IPSO-LSTM			
	Number of iterations	Learning rate	Hidden layer 1	Hidden layer 2
IMF1	200	0.0012	248	20
IMF2	194	0.0025	241	26
IMF3	201	0.0011	244	19
IMF4	198	0.0021	231	21
IMF5	189	0.0039	222	33
IMF6	204	0.0010	235	19
IMF7	195	0.0018	248	20
IMF8	203	0.0041	248	21
Res	206	0.0011	247	19

IV. Analysis Of Experimental Result

A. CEEMDAN decomposition

The original data decomposed by CEEMDAN present a multi-level modal structure [31]. This study effectively decomposes the original bicycle flow data into multiple IMF components and residual terms of different frequencies. Each IMF possesses distinct characteristics in terms of frequency, amplitude, and period. These IMFs are arranged in descending order of frequency, as shown in Fig. 5.

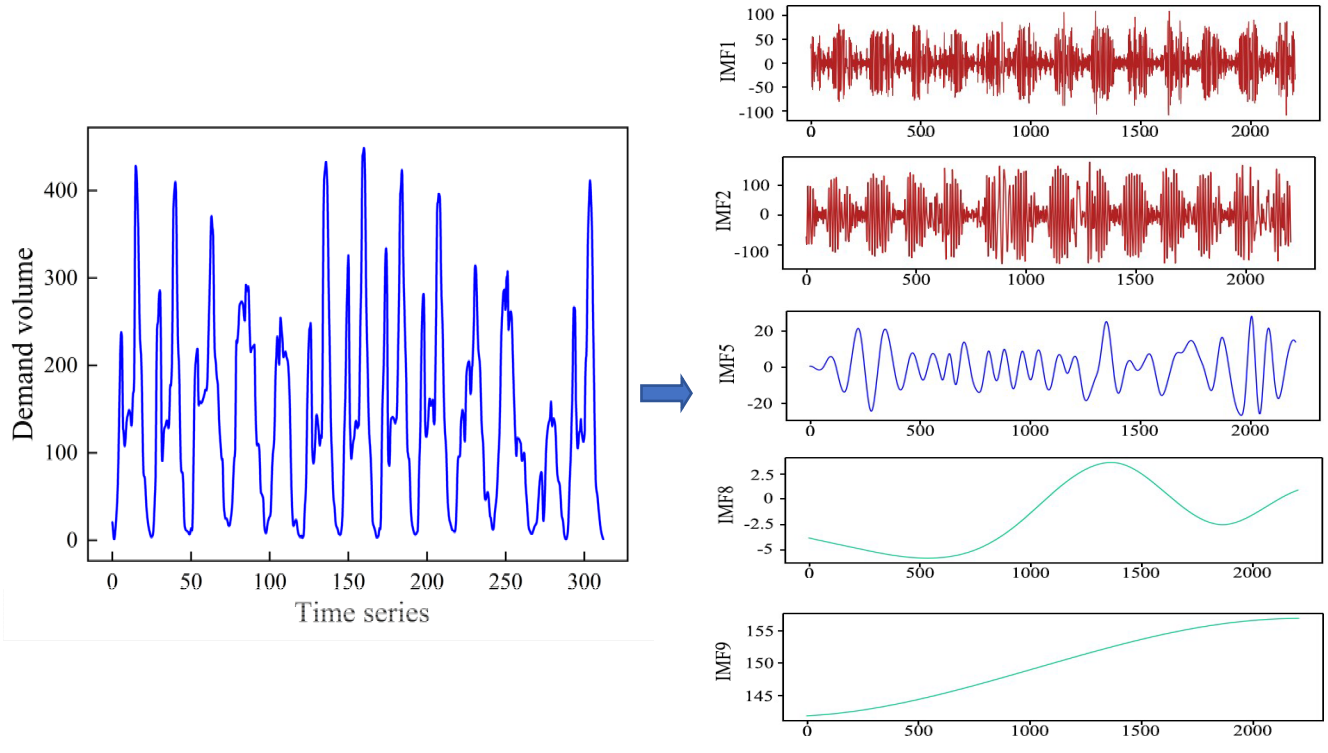

Fig. 5. Bicycle Flow Data CEEMDAN Decomposition

High-frequency IMFs (such as IMF1 and IMF2) primarily manifest as short-term fluctuations. These modes typically reflect noise or short-term fluctuations in bicycle usage, often associated with sudden events, holidays, or weather changes. Such fluctuations are small in amplitude but occur frequently and with significant variability.

Mid-frequency IMFs (such as IMF5 and IMF6) often reflect relatively stable periodic fluctuations. They reveal mid-term trends in the data, such as regular changes in bicycle usage on weekends or weekdays, which may exhibit more pronounced periodic characteristics.

Low-frequency IMFs (e.g., IMF8 and IMF9) primarily capture long-term trend changes. These modes change slowly, have longer periods, and exhibit larger amplitudes, typically revealing long-term trends in the data, such as changes in bicycle usage due to policy changes, population migration, or urban development.

CEEMDAN decomposition effectively separates high-frequency and low-frequency components, reduces modal aliasing, and clearly distinguishes short-term fluctuations from long-term trends, thereby revealing the multi-scale characteristics of shared bicycle data. By introducing adaptive noise, CEEMDAN reduces random noise, improves the stability and accuracy of the decomposition, and provides more precise input data for subsequent model analysis.

B. IMF forecasts and reconstruction

1) IMF forecast analysis

This paper adopts the independent prediction of IMF components (IMF-by-IMF) strategy, which predicts each modal function (IMF) obtained from decomposition separately to more accurately capture the characteristics of changes in different frequency components, as shown in Fig. 6. By decomposing a complex time series into multiple IMF components with distinct characteristic frequencies and predicting them separately, this approach preserves the inherent characteristics of each component while effectively avoiding frequency aliasing. This allows the model to capture dynamic changes within their respective frequency ranges, which are then reconstituted into the original time series signal. This not only improves the prediction accuracy of the model but also facilitates the analysis of the contribution of each frequency component to the overall trend prediction, thereby providing a robust basis for error analysis and model improvement.

By plotting the trend lines of the predicted values and actual values for each IMF, we visually demonstrate the model's prediction performance across different frequency components. We calculate the RMSE, MAE, and R^2 for each IMF using these metrics to quantify the prediction performance of each IMF. as shown in TABLE V. The CEEMDAN-IPSO-LSTM model exhibits varying prediction performance for different frequency components. Overall, as the IMF frequency decreases, the RMSE and MAE show a decreasing trend, while the R^2 gradually approaches 1, indicating that the model predicts low-frequency components more accurately with smaller errors.

The prediction errors in the high-frequency components

(IMF1 and IMF2) are relatively small, with RMSE values of 81.3 and 62.5, respectively, and MAE values of 35.1 and 30.4, respectively. The coefficient of determination R^2 is relatively high (0.865 and 0.914), but there is still some deviation.

The prediction performance of the mid-frequency component (IMF4 and IMF5) improved, with RMSE and MAE of 56.1/24.9 and 42.3/26.1, respectively, and the coefficient of determination significantly increased to 0.954 and 0.987, indicating that the model has a strong ability to capture mid-frequency fluctuations.

The prediction performance of the low-frequency component (IMF8 and IMF9) was optimized, with RMSE gradually decreasing to 28.9 and MAE reaching a minimum of 18.2. The coefficient of determination R^2 approached 1 (0.986 to 0.991), indicating that the model performs exceptionally well in predicting long-term trends with minimal error.

TABLE V
EVALUATION OF PREDICTION PERFORMANCE

IMF	RMSE	MAE	R^2
IMF1	62.3	35.1	0.865
IMF2	60.5	30.4	0.914
IMF3	56.1	24.9	0.937
IMF4	42.3	26.1	0.954
IMF5	27.1	18.2	0.987
IMF6	31.8	19.3	0.984
IMF7	32.2	20.4	0.986
IMF8	30.1	21.5	0.986
IMF9	28.9	18.6	0.991

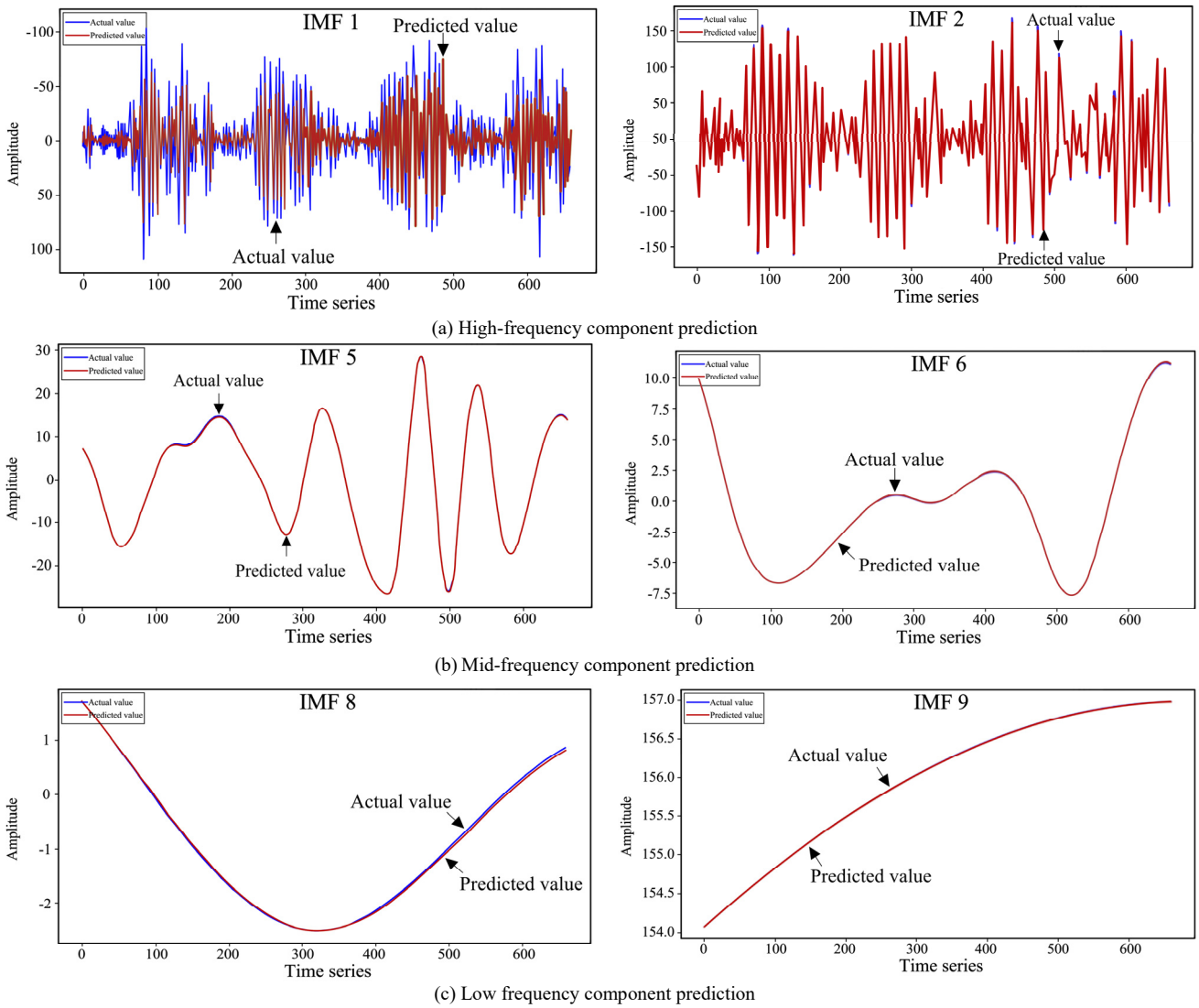

Fig. 6. Component-wise Independent Prediction (IMF-by-IMF) Strategy Diagram

As is evident from the table, the model demonstrates a relatively minor error in predicting high-frequency short-term fluctuations. This implies that it possesses a certain degree of adaptability to short-term fluctuations and local characteristics, and showcases excellent robustness when processing rapidly varying signals. The model exhibits remarkable performance in predicting medium-frequency and low-frequency components, particularly in accurately capturing long-term trends. Moreover, as the frequency diminishes, the prediction error decreases, and the coefficient of determination R^2 approaches unity, indicating that the model has a robust trend-capturing ability.

In summary, the CEEMDAN-IPSO-LSTM model demonstrates good balance when dealing with signal components of different frequencies: it can accurately predict short-term fluctuations and effectively capture medium- and long-term trends. This adaptability to signals across the entire frequency range provides a solid foundation for the model's wide application and also provides a clear direction for further improving prediction accuracy and optimizing the model.

2) IMF forecast results reconstructed

This paper adopts an independent prediction strategy for each component (IMF-by-IMF), in which each IMF and residual term is separately predicted by the prediction model, then recombined to form the overall prediction result. At each time *t*, all IMF prediction values and residual terms corresponding to the prediction results at that time are added together to obtain the reconstructed value at that time. The reconstruction formula is as follows:

$$\hat{X}(t) = \hat{IMF}_1(t) + \hat{IMF}_2(t) + \ldots + \hat{IMF}_n(t) + \hat{R}(t) \quad (17)$$

In the equation, $\hat{X}(t)$ is the reconstruction prediction value at time *t*, $\hat{IMF}_{i(t)}$ is the prediction value of the *i*-th IMF component at time *t*, and $\hat{R}(t)$ is the residual term at time *t*.

By connecting the reconstructed values at each time point into a complete time series, the overall reconstructed prediction result is obtained. The reconstructed prediction values not only contain the characteristics of each IMF component but also capture the long-term trend information from the residual term, thereby reflecting the comprehensive changes of the original data across various time scales.

C. Model comparison and evaluation

To further understand the performance advantages of the CEEMDAN-IPSO-LSTM model in the urban shared bicycle demand forecasting scenario, it needs to be compared and analyzed with various benchmark deep learning models, especially through comparison with the LSTM, PSO-LSTM, IPSO-LSTM, and CEEMDAN-LSTM models. This will clearly demonstrate the synergistic effect of CEEMDAN decomposition and the IPSO algorithm and quantify the performance improvement, as shown in Fig. 7.

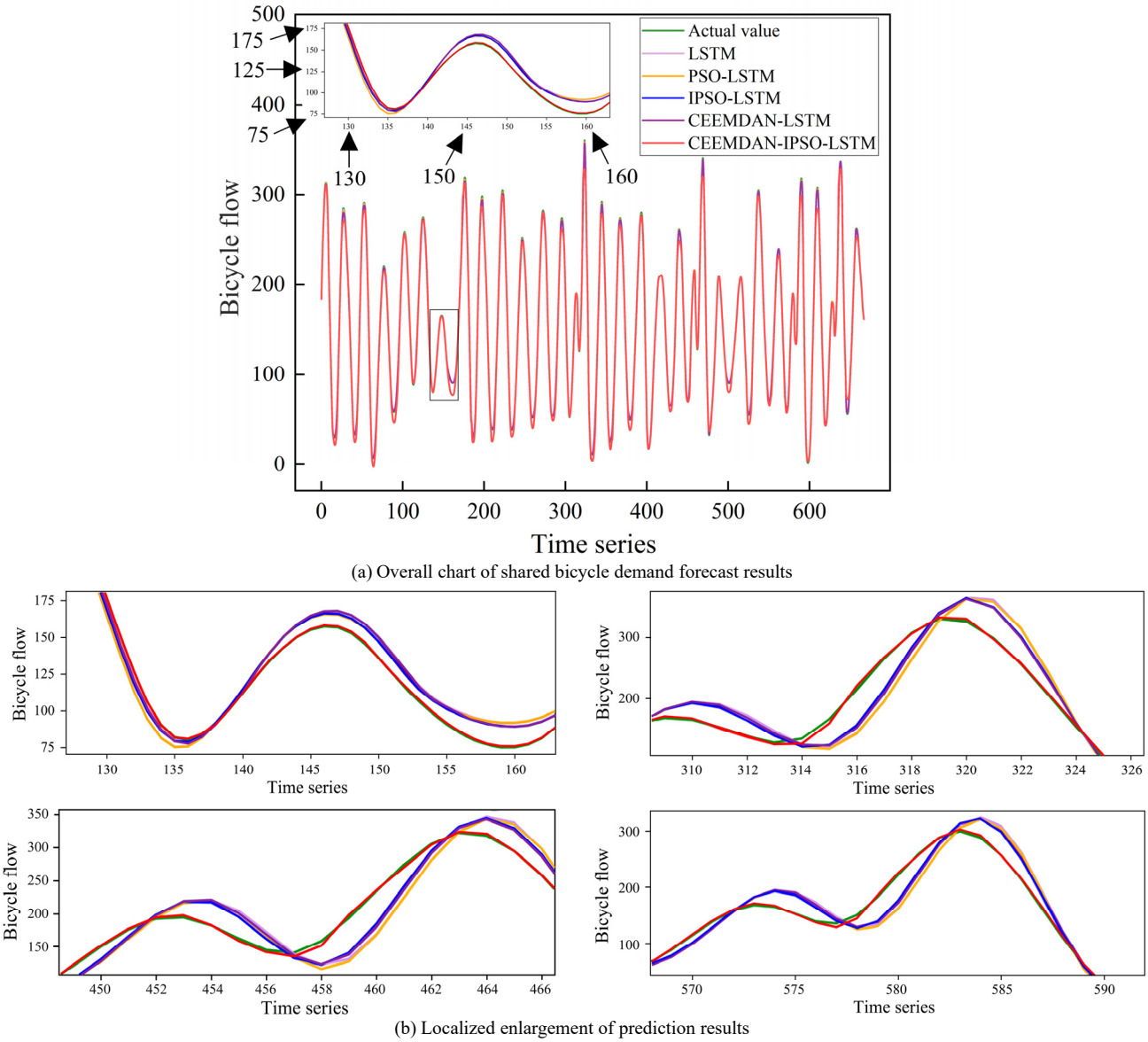

(a) Overall chart of shared bicycle demand forecast results

(b) Localized enlargement of prediction results

Fig. 7. Performance Comparison Analysis Chart of Baseline Models

TABLE VI
EVALUATION METRICS FOR FIVE MODELS

Model	Evaluation Criteria			
	MAE	RMSE	MAPE/%	R^2
LSTM	34.81	50.39	20.19	0.859
PSO-LSTM	29.95	43.12	16.47	0.913
IPSO-LSTM	25.36	35.61	14.36	0.931
CEEMDAN-LSTM	26.78	37.21	18.91	0.952
CEEMDAN-IPSO-LSTM	20.47	30.84	10.56	0.995

Model prediction results show that the overall trends of the five models are generally consistent with the actual values, especially in terms of the peak and trough positions of the time series, where all models accurately capture the trends in bicycle flow. However, there are significant differences among the models in terms of handling local fluctuations, capturing complex changes, and predicting long-term trends. Compared to other models, it not only demonstrates excellent robustness and predictive capability in handling nonlinear fluctuations in time-series data but also effectively eliminates noise interference, providing reliable support for high-precision shared bicycle scheduling. Therefore, the CEEMDAN-IPSO-LSTM model exhibits significant advantages in practical applications, particularly in bicycle flow prediction scenarios with complex fluctuation characteristics.

By comparing the convergence curves of the five models over 100 training cycles, we can specifically evaluate the convergence speed and final performance of each model. As shown in Fig. 8, the CEEMDAN-IPSO-LSTM model exhibits the best convergence performance. The convergence curve of this model drops rapidly in the early stages, indicating extremely fast initial convergence, and remains highly stable throughout the training process, with the final loss value significantly lower than that of other models. This result indicates that the combination of CEEMDAN's signal decomposition method and IPSO's optimization strategy not only significantly accelerates the model's convergence speed but also effectively improves prediction accuracy while significantly reducing potential fluctuations during the training process.

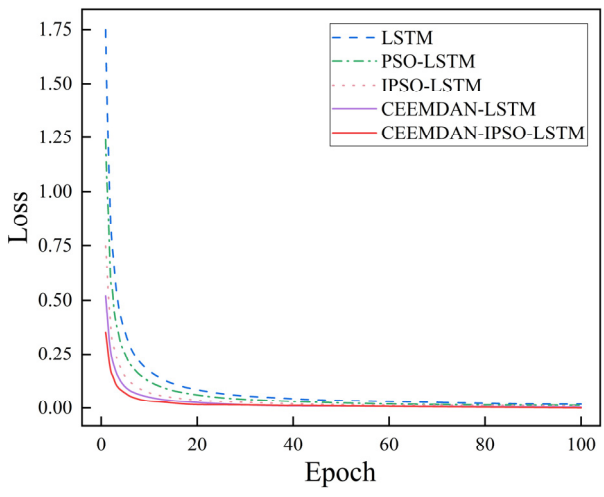

Fig. 8. Convergence curve comparison of models

Through the comparison of the residuals of the five models, a residual comparison plot was constructed. The scatter plot shows the correspondence between the predicted values and the actual values of each model, while the box plot further reveals the distribution characteristics of the residuals of different models. As presented in Fig. 9, there are significant differences among the models in terms of prediction accuracy and stability. The residuals of the CEEMDAN-IPSO-LSTM model nearly coincide with the zero line, and the residual range is the narrowest, indicating a high degree of consistency between its predicted and actual values, thereby demonstrating exceptional prediction accuracy and stability. This implies that the integrated strategy of multi-model optimization and time series decomposition enables this model to attain optimal prediction performance.

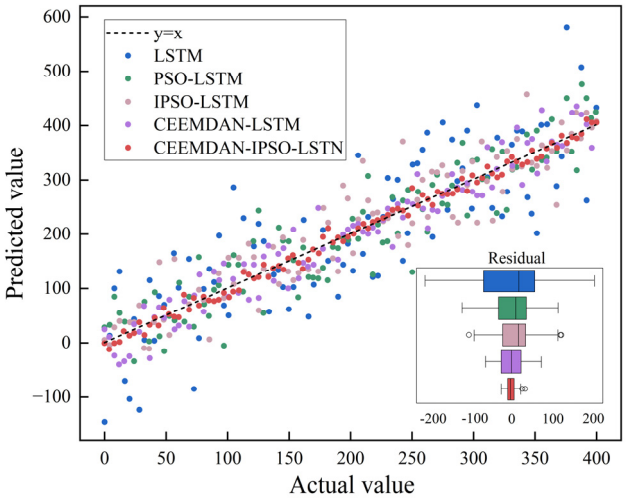

Fig. 9. Residual comparison analysis of five models

V. CONCLUSION

In order to solve the demand problem of shared bicycles, this study utilizes the New York shared bicycle dataset to construct the CEEMDAN-IPSO-LSTM combined prediction model. This model effectively resolves two crucial problems in the demand prediction of shared bicycles: eliminating data noise and optimizing neural network parameters. Moreover, an optimization strategy integrating CEEMDAN decomposition and IPSO optimization is proposed.

Through the decomposition of time series data into multiple modal functions and residual terms, CEEMDAN effectively reduces noise interference. Specifically, the IPSO further enhances the predictive performance of the model by dynamically optimizing the key parameters of the LSTM model. The proposed prediction model adopts a multivariate forecasting strategy, integrating diverse factors from real-world scenarios, including weather types, rainfall amounts, wind speeds, and holidays. This approach effectively validates the model's superiority in dealing with complex multivariate time-series data.

By conducting a comprehensive comparison of diverse experimental results, we validate the superiority and efficacy of the model, which is expected to further enhance the prediction accuracy. This research offers novel perspectives and methodologies for tackling intricate forecasting challenges within urban transportation systems.

It holds substantial application value and potential for the advancement of intelligent transportation systems and the refined management of shared mobility services.

REFERENCES

[1] S. Wang, J. Zhang, L. Liu and Z. Duan, "Bike-Sharing-A new public transportation mode: State of the practice & prospects," in *2010 IEEE International Conference on Emergency Management and Management Sciences*, pp. 222–225, 2010.

[2] X. Luo, W. Gu and W. Fan, "Joint design of shared-bike and transit services in corridors," *Transportation Research Part C: Emerging Technologies*, vol. 132, p. 103366, 2021.

[3] N. Gast, G. Massonnet, D. Reijsbergen and M. Tribastone, "Probabilistic Forecasts of Bike-Sharing Systems for Journey Planning," in *Proceedings of the 24th ACM International on Conference on Information and Knowledge Management*, Melbourne Australia: ACM, pp. 703–712, 2015.

[4] A. A. Campbell, C. R. Cherry, M. S. Ryerson and X. Yang, "Factors influencing the choice of shared bicycles and shared electric bikes in Beijing," *Transportation Research Part C: Emerging Technologies*, vol. 67, pp. 399–414, 2016.

[5] F. Lin, Y. Yang, S. Wang, Y. Xu, H. Ma and R. Yu, "Urban public bicycle dispatching optimization method," *PeerJ Computer Science*, vol. 5, p. 224, 2019.

[6] N. Guo, R. Jiang, Q.-Y. Hao, S.-Q. Xue and M.-B. Hu, "Bicycle flow dynamics on wide roads: Experiment and modeling," *Transportation Research Part C: Emerging Technologies,* vol. 125, p.103012, 2021.

[7] Y. Wei, S. Sun, J. Ma, S. Wang and K. K. Lai, "A decomposition clustering ensemble learning approach for forecasting foreign exchange rates," *Journal of Management Science and Engineering*, vol. 4, no. 1, pp. 45–54, 2019.

[8] Y. Lv, Y. Duan, W. Kang, Z. Li and F.Y. Wang, "Traffic Flow Prediction With Big Data: A Deep Learning Approach," *IEEE Trans. Intell. Transport. Syst*, vol.16, no.2, pp. 1–9, 2014

[9] S. M. Al-Selwi, M. F. Hassan, S. J. Abdulkadir, A. Muneer, E. H. Sumiea, A. Alqushaibi and M. G. Ragab, "RNN-LSTM: From applications to modeling techniques and beyond—Systematic review," *Journal of King Saud University - Computer and Information Sciences*, vol. 36, no. 5, p. 102068, 2024.

[10] M. Cai, Y. Wang, S. Wang, R. Wang, L. Cheng and M. Tan, "Prediction-Based Seabed Terrain Following Control for an Underwater Vehicle-Manipulator System," *IEEE Trans. Syst. Man Cybern, Syst*, vol. 51, no. 8, pp. 4751–4760, 2021.

[11] X. Yuan, L. Li and Y. Wang, "Nonlinear Dynamic Soft Sensor Modeling With Supervised Long Short-Term Memory Network," *IEEE Trans. Ind. Inf*, vol. 16, no. 5, pp. 3168–3176, 2020.

[12] Y. Huang, Y. Huang, J. Li, Y Li, R. Lin, J. Wu, L. Wang and R. Chen, "An Improved Hybrid CNN-LSTM-Attention Model with Kepler Optimization Algorithm for Wind Speed Prediction," *Engineering Letters*, vol. 32, no. 10, pp. 1957-1965, 2024.

[13] S. Qiao, N. Han, H. Li, G. Yuan, T. Wu, Y. Peng, H. Cai and J. Huang, "A three-in-one dynamic shared bicycle demand forecasting model under non-classical conditions," *Applied Intelligence*, vol. 54, no. 17–18, pp. 8592–8611, 2024.

[14] Z. Wang, Q. Zhao, L. Wang, W. Xiu, and Y. Wang, "Bike-Sharing Travel Demand Forecasting via Travel Environment-Based Modeling," *Applied Sciences*, vol. 14, no. 16, 2024.

[15] J. Feng, H. Liu, J. Zhou and Y. Zhou, "A Spatial-Temporal Aggregated Graph Neural Network for Docked Bike-sharing Demand Forecasting," *ACM Trans. Knowl. Discov. Data*, vol. 18, no. 9, p. 232:1-232:27, 2024.

[16] "Framework for hourly demand forecasting of bike-sharing stations: case study of the four main gate areas in Seoul: International Journal of Urban Sciences: Vol 28 , No 4 - Get Access." Accessed: Apr. 28, 2025. [Online]. Available: https://www.tandfonline.com

[17] Y. Shi, L. Zhang, S. Lu and Q. Liu, "Short-Term Demand Prediction of Shared Bikes Based on LSTM Network," *Electronics*, vol. 12, no. 6, p. 1381, 2023.

[18] F. Huang, S. Qiao, J. Peng and B. Guo, "A Bimodal Gaussian Inhomogeneous Poisson Algorithm for Bike Number Prediction in a Bike-Sharing System," *IEEE Trans. Intell. Transport. Syst*, vol. 20, no. 8, pp. 2848–2857, 2019.

[19] H. I. Ashqar, M. Elhenawy, H. A. Rakha and L. House, "Quality of Service Measure for Bike Sharing Systems," *IEEE Trans. Intell. Transport. Syst*, vol. 23, no. 9, pp. 15841–15849, 2022.

[20] C. Ma and T. Liu, "Demand forecasting of shared bicycles based on combined deep learning models," *Physica A: Statistical Mechanics and its Applications*, vol. 635, p. 129492, 2024.

[21] B. Lindemann, T. Müller, H. Vietz, N. Jazdi, and M. Weyrich, "A survey on long short-term memory networks for time series prediction," *Procedia CIRP*, vol. 99, pp. 650–655, 2021.

[22] M. E. Torres, M. A. Colominas, G. Schlotthauer and P. Flandrin, "A complete ensemble empirical mode decomposition with adaptive noise," in *2011 IEEE International Conference on Acoustics, Speech and Signal Processing (ICASSP)*, pp. 4144–4147, 2011.

[23] X. Liu, R. Lu, N. Yang, Y. Xiao and A. Jadoon, "Research on DC Bias Saturation Characteristics of Transformer Combining CEEMD and FuzzyEn Method," *Engineering Letters*, vol. 32, no. 10, pp. 1888-1900, 2024.

[24] J. T. Connor, R. D. Martin,and L. E. Atlas, "Recurrent neural networks and robust time series prediction," *IEEE Trans. Neural Netw*, vol. 5, no. 2, pp. 240–254, 1994.

[25] S. Hou and Z. Wang, "Weighted Channel Dropout for Regularization of Deep Convolutional Neural Network," *AAAI*, vol. 33, no. 01, pp. 8425–8432, 2019.

[26] T. M. Shami, A. A. El-Saleh, M. Alswaitti, Q. Al-Tashi, M. A. Summakieh and S. Mirjalili, "Particle Swarm Optimization: A Comprehensive Survey," *IEEE Access*, vol. 10, pp. 10031–10061, 2022.

[27] R. Wang, K. Hao, L. Chen, T. Wang and C. Jiang, "A novel hybrid particle swarm optimization using adaptive strategy," *Information Sciences*, vol. 579, pp. 231–250, 2021.

[28] K. Greff, R. K. Srivastava, J. Koutnik, B. R. Steunebrink and J. Schmidhuber, "LSTM: A Search Space Odyssey," *IEEE Trans. Neural Netw. Learning Syst*, vol. 28, no. 10, pp. 2222–2232, 2017.

[29] Y. Xu, C. Hu, Q. Wu, S. Jian, Z. Li, Y. Chen, G. Zhang, Z. Zhang and S. Wang, "Research on particle swarm optimization in LSTM neural networks for rainfall-runoff simulation," *Journal of Hydrology*, vol. 608, p. 127553, 2022.

[30] E. D. Bobobee, S. Wang, P. Takyi-Aninakwa, C. Zou, E. Appiah and N. Hai, "Improved particle swarm optimization–long short-term memory model with temperature compensation ability for the accurate state of charge estimation of lithium-ion batteries," *Journal of Energy Storage*, vol. 84, p. 110871, 2024.

[31] I. Karijadi and S.-Y. Chou, "A hybrid RF-LSTM based on CEEMDAN for improving the accuracy of building energy consumption prediction," *Energy and Buildings*, vol. 259, p. 111908, 2022.